Applied Chemistry Today **19(73)** (2025) 59-72

Semnan University

Applied Chemistry Today

Journal homepage: https://chemistry.semnan.ac.ir/

ISSN: 2981-2437

Research Article

Fluorescent UV-curable Polyurethane Acrylate Nanocomposite Coatings Strengthened with Carbon Quantum Dots: Preparation and Investigation of UV-blocking and Anti-Corrosive Properties

Abbas Madhi[a,*], Behzad Shirkavand Hadavand[b,*], Mohammad Hassan Madhi[c], Zahra Rahmani[b]

[a]*Color Technology Incubator, Institute for Color Science and Technology, 1668814811, Tehran, Iran*
[b]*Department of Resin and Additives, Institute for Color Science and Technology, 1668814811, Tehran, Iran*
[c]*Faculty of Art and Architecture, Islamic Azad University West Tehran Branch,1468763785, Tehran, Iran*

PAPER INFO

Article history:
Received: 26/Feb/2024
Revised: 26/Apr/2024
Accepted: 03/Jun/2024

Keywords:
Bio-based,
Polyurethane acrylate,
Fluorescent coatings,
UV-blocking property,
Anti-corrosive behavior.

ABSTRACT

Most polymers exposed to UV radiating from the sun deteriorate and lose their mechanical features. Polymer coatings are generally used for protection of metal surfaces against corrosive factors. Thus, production of coatings blocking the sunlight UV rays is necessary to protect the metal surfaces. This work mainly focuses on synthesis of fluorescent bio-based UV-curable polyurethane acrylate (PUA) and studies the changes occurred in the various specifications of these coatings resulted from adding carbon quantum dots (CQDs). To synthesize PUA oligomer, castor oil was applied as a natural and biocompatible substance instead of chemical polyols. By pyrolysis of the starch and water blend, CQDs were synthesized using microwave-assisted method. To characterize the synthesized coatings and to analyze the reinforcing effect of CQDs on the resultant nanocomposite, electroscopic methods were utilized. Adding CQDs 0.5 wt% to PUA resin resulted in improvement of adhesion strength and thermal stability in PUA/CQDs (0.5 wt%) coating compared to PUA (pure) coating. With exposing PUA/CQDs to UV rays, blue fluorescence was emitted and strong absorption bands also appeared in all of the UV regions. Most of the UV rays passed through the PUA film, while PUA/CQDs blocked higher than 99% of UV radiation. Results from salt spray and EIS tests confirmed that resistance to corrosion was improved in PUA/CQDs coating versus the pure coating.

DOI: https://doi.org/10.22075/chem.2024.33360.2253

[*]**Corresponding authors:** Professor of organic chemistry. *E-mail address: shirkavand@icrc.ac.ir*

How to cite this article: Madhi, A., Shirkavand Hadavand, B., Madhi, M. H., & Rahmani, Z. (2025). Fluorescent UV-curable Polyurethane Acrylate Nanocomposite Coatings Strengthened with Carbon Quantum Dots: Preparation and Investigation of UV-blocking and Anti-Corrosive Properties. *Applied Chemistry Today*, **19(73)**, 59-72. (in Persian)

1. Introduction

Polyurethanes (PUs) have recently drawn lots of attention due to unequalled properties. Polyurethanes hold optimal specifications such as toughness, flexibility, thermal stability, chemical resistance, good mechanical characteristics and endurance to corrosive causes [1, 2]. PUs are greatly used in industry and hence are applied in production of coating films, adhesives, foams, sealants, cars parts, airplane parts, electronic industry and so forth [3-5]. Polyurethanes are usually prepared through a reaction between diisocyanate and diols or polyols.

Nowadays, UV-curable coatings play a significant role in various industries. Curing mechanism of polymer nanocomposites with UV rays can be esteemed a useful way that can preserve the environment regarding lower temperature for curing, removing hazardous organic solvents, and great efficiency [6, 7]. In this mechanism, polymerization occurs and during this, double bonds-contained monomers and oligomers like urethane acrylate resin become a crosslinking owing to a photo-initiator existence and a brief UV radiation [8, 9]. A lot of attention is drawn to the polymers derived from renewable resources and therefore, vegetable oils production and development to be employed in polymers is a notable goal of chemical industries [10]. Because, these substances are non-poisonous in addition to renewability and biodegradability. Castor oil as a ricinoleic acid resource (85%-95%) possesses hydroxyl functional groups by which could optimally react with various chemical groups [11, 12]. Besides, castor oil could be a good substitute for some petroleum-based polyols [13].

Recently, use of polymer substances in industries has increasingly expanded. Fast optical degradation of polymer coatings under UV from sunlight is common [14]. The polymer constructions exposure to UV radiation results in optical destruction, weakening of mechanical properties, changes in chemical features as well as economic and environmental implications [15, 16]. Almost, all of the polymers and polymer composites require UV-absorbent additives and optical stabilizers. So, it is necessary to find a solution for reducing or avoiding the harms arising from optical decomposition of polymer coatings [17].

Carbon quantum dots (CQDs) are a kind of zero-dimensional carbon nanoparticles diameter of which is less than 10 nm [18]. CQDs are produced through various mechanisms, for example, pyrolysis, electrochemistry, and acid oxidation of carbonous resources such as graphite, starch, citric acid, urea and others [19, 20]. CQDs have specifications like biocompatibility, solubility in water and low toxicity. Excellent optical features such as absorption of UV rays and fluorescence emission are the reasons that make the use of CQDs an acceptable idea to synthesize fluorescent polymers holding ability of resistance against harmful UV rays [21, 22]. Additionally, owing to solubility in water and chemical solvents, CQDs as a dependable nanofiller can be used to reinforce different features of polymers including mechanical properties, viscoelastic traits, thermal stability, and resistance against corrosion [23].

Polymer nanocomposites are applied to metal layers as a surface coating to avoid them from corrosion damage and reduce economic and environmental losses [24]. Efficiency and durability of the anti-corrosive effects of coatings depend on some causes such as cross-link density, adhesion power of coating to metal, and type and amount of filler particles [25]. Polymer nanocomposites create a protective coating on steel surfaces and reduce the speed of corrosion process. Anti-corrosive coatings are widely usable for petroleum, petrochemical, gas and power plant industries in order to protect the installations of these industries from environmental

corrosive factors and prevent leakage of chemical compounds to environment [26, 27].

There have been several methods in recent years to protect metal surfaces against corrosion. Some studies on this field are as follows: Polyurethane coating has been used to protect the steel surfaces applied in historical constrictions from weathering and corrosion [28]. Polymer coatings such as polyurethane, epoxy and polymer nanocomposites used on surfaces are continuous without any hole and consequently are greatly beneficial compared to former techniques like coloring and greasing [29]. Other study employed polyaniline and polyindole electrical conductor polymers, and a similar work used Schiff bases based on thiosemicarbazide to avoid carbon steel corrosion [30, 31]. In a research work, Ni-W/SiO_2 homogenous coating was put to use to keep copper surfaces from corrosive media, and a similar study was done by use of polyaniline coating via chronopotentiometery method under galvanostatic state [32, 33]. For another research, quality of nickel coating on steel surface was investigated under Watts bath conditions using ethylene glycol or diethylene glycol additives. The findings of the polarization spectra confirmed a great reduction in corrosion intensity in the steel surface coated by nickel in presence of corrosive factors in contrast with the steel surface without nickel coating [34].

Consequently, due to capability of UV absorption and fluorescence emission in the visible wavelength, CQDs could be a fitting candidate to protect the polymer coatings against harmful UV rays [35, 36]. As a nanofiller, CQDs are also able to strengthen the protective coatings of steel surfaces against corrosive factors like dampness, oxygen in the air and chloride ions [37].

In the current study, castor oil as a natural and biocompatible polyol was used to synthesize the PUA-based coatings. Next, the effect of adding CQDs 0.5 wt% to the polymer matrix on thermal stability, adhesion strength, fluorescence properties, blocking of UV rays and resistance to corrosion of the synthesized coatings was reported and discussed.

2. Experimental

2.1. Materials and methods

Castor oil was provided from a local market. Starch, triethanolamine (TEA), dibutyltin dilaurate (DBTDL), acetone, benzophenone and 2-hydroxyethyl methacrylate (HEMA) were bought from a company called Merck. Isophorone diisocyanate (IPDI) and trimethyle propane triacrylate (TMPTA) were prepared from Sigma Aldrich company.

Functional groups of the samples were examined by FTIR device, One Spectrum model, made by Perklin-Elmer. FESEM spectroscopy device (Tuscan Mira3) was used to inspect the morphology and distribution quality of CQDs in PUA matrix. By thermogravimetric analysis, Pyris Diamond model, made by Perkin-Elmer company, thermal stability of the coatings was judged. Pull-off adhesion strength of the coatings was studied on the steel surface via Defelsko tester. Fluorescence response and UV-shielding property of the samples were assessed by Perkin Elmer LS 55 Fluorescence spectrometer, and Specord 250 UV/Vis spectrophotometer. To evaluate the resistance of coatings to corrosion, electrochemical impedance spectroscopy (EIS), CST800E model, and salt spray technique (ASTM B117) were conducted. The samples in a parallel state to each other, without any intersection, with a 30-degree angle to perpendicular line and parallel to the main direction of the salt spraying were exposed to an accelerated corrosive environment in the salt spray device at 35 °C. These samples were indirectly sprayed with Sodium chloride 5 wt% solution in distilled water with a pH of 6.5-7.2. Before placing the samples in the device, by a sharp scratcher, a 5 cm scratch was made in the middle of the samples

along the length so that the base metal appeared in the scratched region. Before spraying the salt, the samples' back and edges were covered with beeswax-colophony mixture.

In order to conduct EIS testing, an area of 1×1 cm^2 was determined on the samples and the rest of them were covered by beeswax-colophony mixture. After exposure to a 24-hour salt spraying, and following 240 hours floating in sodium chloride 3.5% solution in a frequency range of 10 mHz to 10 kHz, with 10 mV perturbation amplitude using a three electrodes system including the working electrode (the samples), the Ag/AgCl reference electrode to control the applied potential and platinum auxiliary electrode, EIS testing was carried out to flow of current. The resulted EIS graphs were fitted using ZView 3.1 software.

magnetic stirrer and was put aside to be used for the next step.

To synthesize PUA oligomer, in the first place, 5.5 g IPDI, 7.75 g castor oil, 15 mL acetone and 0.3 mL DBTDL as a catalyst were poured into a double neck balloon having a nitrogen inlet, and a condenser. Then, 3.25 g HEMA was added in drops to the mixture and agitated for a 90-minute time at 80 °C. Here, PUA oligomer was obtained. The synthesized PUA was evenly poured into two beakers and each of both was loaded by 1.75 g TMPTA.

CQDs dissolved in DMF mixture was added to one of these beakers and stirred by a magnetic stirrer with 900 rpm for 1 hour until CQDs particles were homogenously dispersed throughout the resin matrix. Afterwards, 0.03 g TEA (co-initiator) and 0.03 g benzophenone (photo-initiator) were added to each beaker. These mixtures were agitated for 3 minutes at 25 °C. Next, many 0.3 mm thick films were molded. To verify the removal of solvent, the molds remained at 25 °C for 10 h. In the end, the molds were exposed to a UV lamp (Hg, 1000W) and curing process of the films was fulfilled. The prepared films were named PUA (blank) and PUA/CQDs (0.5 wt%). Figure 1 exhibits the synthesis steps of PUA/CQDs nanocomposite coating.

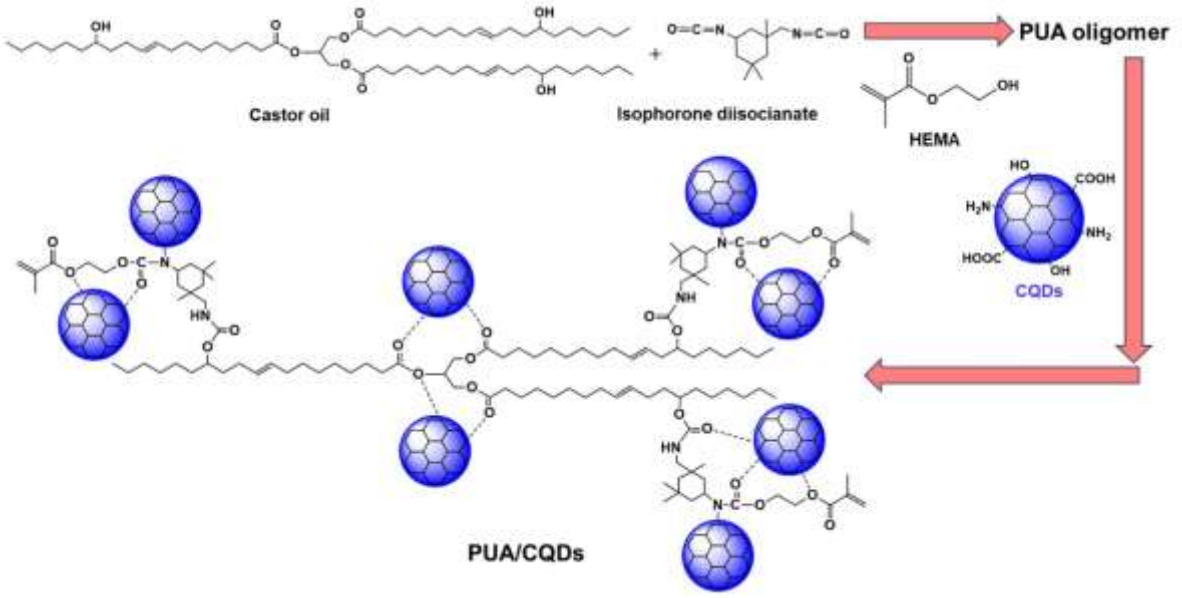

Fig. 1. Synthesis steps of PUA/CQDs films.

2.2. Synthesis of the coatings

Through pyrolysis of the starch-water blend, CQDs were synthesized by microwave-assisted method. In a previous work, characterization and synthesis mechanism of CQDs were discussed [38]. In a small beaker, 0.05 g CQDs dissolved in 2 mL DMF and the resultant compound was stirred for 15 minutes by an ultrasonic probe and then, for 1 hour by a

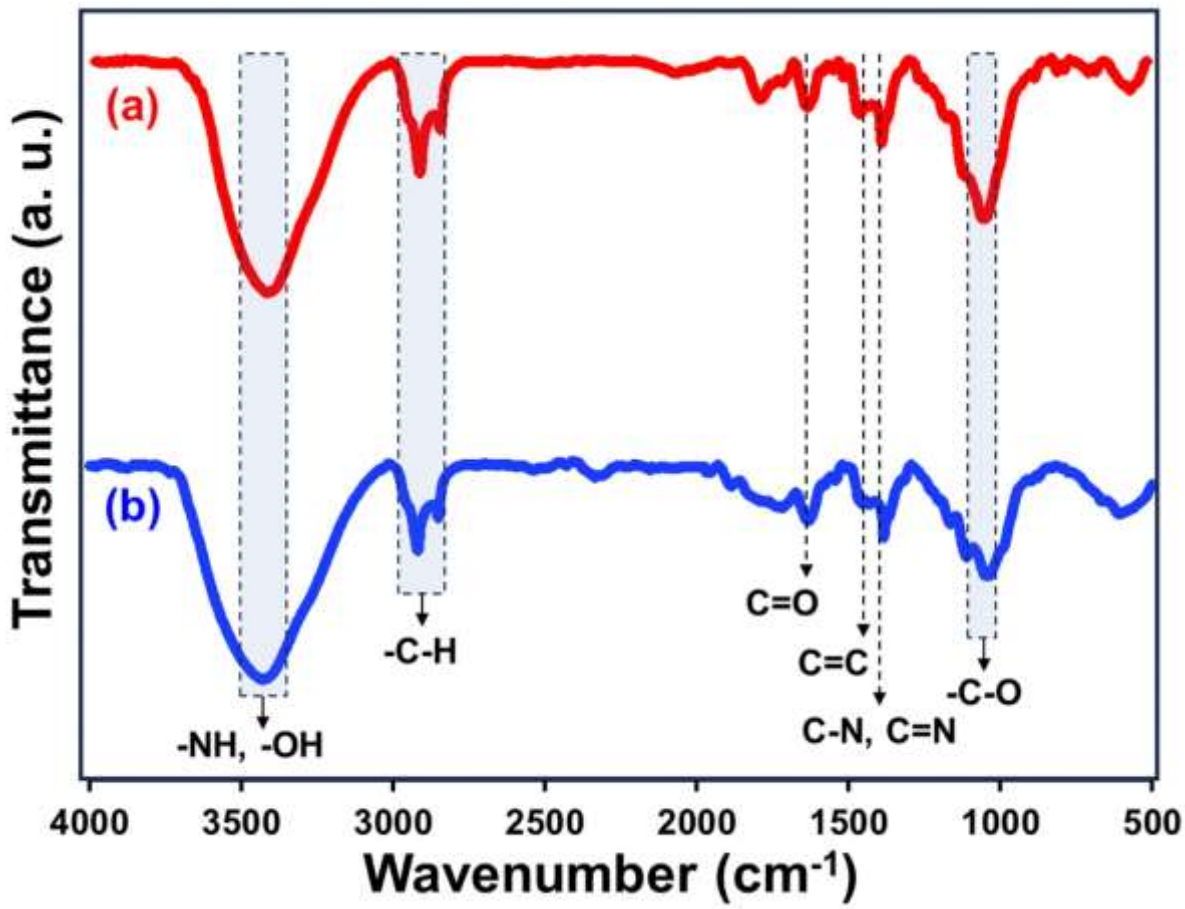

Fig. 2. FTIR spectra of PUA and PUA/CQDs films.

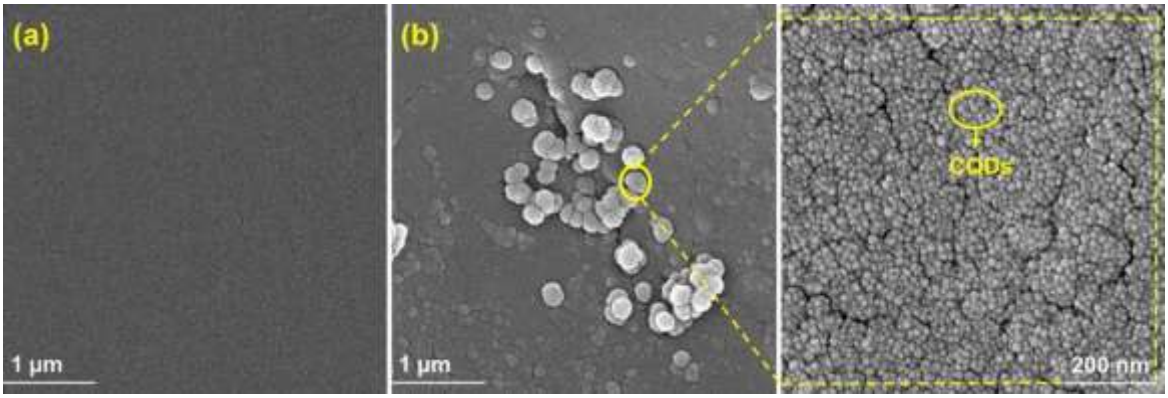

Fig. 3. FESEM micrographs of (a) PUA and (b) PUA/CQDs films.

3. Results and Discussion

3.1. Characterization

Figure 2 discloses FTIR spectra for characterization of functional groups existent in PUA and PUA/CQDs films. The chief absorption bands for PUA consist in: 3427, 2931, 1703 and 1046 cm^{-1} respectively pertain to stretch vibrations of -NH/-OH, -C-H, C=O and -O-. The peak at 1539 cm^{-1} belongs to -NH bends. Loading CQDs to the polymer matrix and PUA/CQDs formation made some changes on the FTIR spectrum that include the shifts in absorption bands [39, 40]. The major observed peaks for PUA/CQDs are 3433, 2943, 1716 and 1633 cm^{-1}, respectively provoked by -

NH/-OH, -C-H, C=O and C=C. Moreover, the bands appeared at 1419 and 1048 cm^{-1} are induced by -CN and C-O- [41].

Surface morphology of the PUA and PUA/CQDs films was assessed by FESEM micrographs. Figure 3(a) witnesses that PUA film surface is plain lacking fracture and any extra particle. Existence of CQDs and dispersion manner of these particles throughout the polymer matrix in PUA/CQDs film surface is clearly observable in Figure 3(b). Uniform dispersion throughout the film and non-agglomeration of the particles offers a good match between CQDs and polyurethane acrylate matrix. Accordingly, one can expect that uniform distribution of particles and agreement of CQDs with polymer matrix lead the optical features, thermal stability and resistance to corrosion to be improved in PUA/CQDs nanocomposite film.

3.2. Thermal stability

TGA curves of PUA and PUA/CQDs films are illustrated in Figure 4. Adding CQDs to the polymer matrix improved thermal stability in PUA/CQDs film compared to PUA film. As TGA curves suggest, weight loss of the samples occurred in 3 steps. Weight loss at 100-200 °C could arise from evaporation of the residual solvent and unreacted substances. At about 200-300 °C, TGA curves slope descends and weight loss of the samples is more obvious confirming an increase in molecular motion and polymer chains loosening. Above 300 °C temperatures, TGA curves slope descends sharply so as this descending is intensified at 350-450 °C signifying polymer thermal decomposition and disconnection between CQDs and polymer chains. The samples weight loss values for PUA and PUA/CQDs films at 300 to 450 °C are represented in Table 1. Growth of temperature results in creation of free radicals, separation of polymer chains and decomposition of polymer [42]. By adding CQDs to the polymer matrix, a charcoal layer is formed on its surface and oxygen absorption ceases for burning process of the PUA/CQDs, and in light of this mechanism, CQDs play thermal protector role for polymer chains. As a result, degradation of nanocomposite coating occurs at higher temperatures and this way, thermal stability grows.

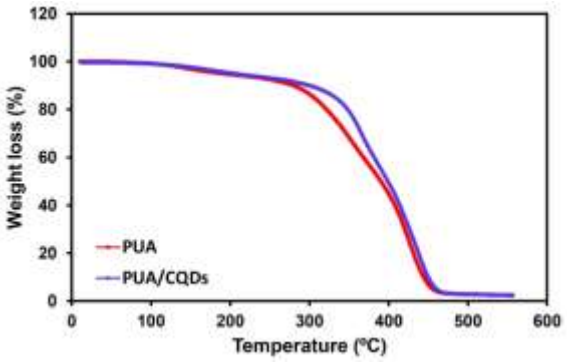

Fig. 4. TGA curves of PUA and PUA/CQDs films.

Table 1. Weight loss percentages for PUA and PUA/CQDs films.

Temperature (°C)	Samples	
	PUA Loss weight (%)	**PUA/CQDs** Loss weight (%)
300	86.42	90.05
350	68.22	79.17
400	44.28	49.54
450	6.91	10.21

3.3. Pull-off adhesion strength

Adhesion strength in the steel-coating interface was evaluated after surface operations. Figure 5 indicates the evaluation results of adhesion strength performance. Adhesion strength of the PUA film was lower than that of PUA/CQDs film in a manner that fracture mode in the substrate for PUA-steel interface was shallow and in contrast, by CQDs concentration increase in polymer matrix, fracture mode in the steel-PUA/CQDs interface gradually turned from shallow to cohesive and the fracture place became deeper. Adhesion strength in the steel-coating interface for PUA/CQDs is higher than that for PUA. Findings approved that by adding CQDs 0.5 wt% to the polymer matrix, adhesion strength in the surface between steel and the film intensifies. So that the adhesion strength of PUA/CQDs increased 0.76 MPa against the blank sample. The reason is

that adhesion bonds are often a kind of physical interactions that cause an increase in adhesion strength by means of hydrogen bonds, mechanical interlocking and van der Waals forces [43]. Homogenous scatter of CQDs throughout the matrix and constitution of chemical and physical interactions in the steel-PUA/CQDs interface heighten the adhesion strength.

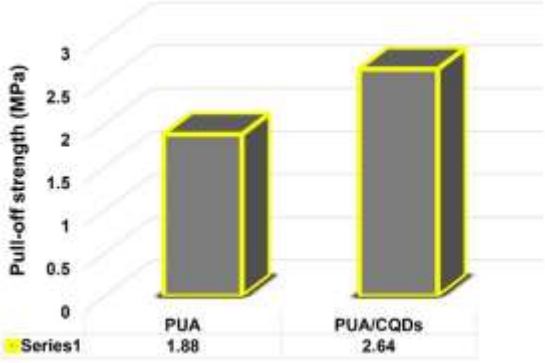

Fig. 5. Pull-off adhesion strength for PUA and PUA/CQDs coatings.

3.4. Fluorescent and UV-blocking properties of coatings

Fluorescence spectra of the coatings are shown in Figure 6. Fluorescence specification of the samples is influenced by CQDs existence, because PUA evinced no noteworthy fluorescence emission in the excitation wavelength at 365 nm, while PUA/CQDs nanocomposite excited by the same wavelength started to emit strong blue fluorescence with 470 nm wavelength. PUA/CQDs fluorescence response could be attributed to the electron excitement of functional groups existing on the CQDs edges such as C=O, C=C and -CN that create visible radiations [44]. Absorption spectra of UV-visible PUA and PUA/CQDs films are depicted in Figure 7. PUA film offers a very weak absorption in the UV region in a way that it could be ignored. However, PUA/CQDs film in UV region evinces strong absorption. The absorption bands observed at 225 nm and 280 nm are ascribed to π→π* transferring in C=C and C=N bonds, and the absorption band at 365 nm is claimed to be led by n→π* relocating in C-N and C=O bonds [45].

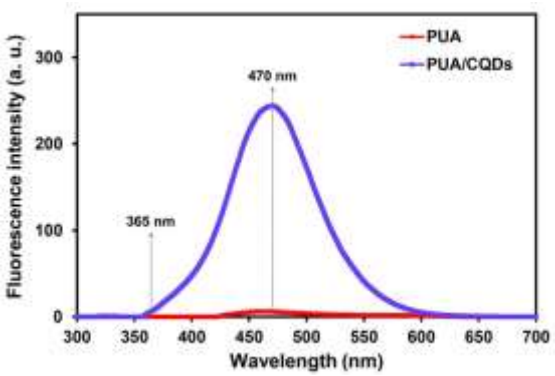

Fig. 6. FL spectra for PUA and PUA/CQDs coatings.

Protective manner of PUA and PUA/CQDs films exposed to UV light in all regions of UVC, UVB and UVA was studied. UV passing values through PUA and PUA/CQDs films in UVB and UVA areas were figured using equations 1 and 2 [46, 47]:

$$\text{UVB blocking } (\%) = 100 - \frac{100 \int_{280}^{320} T(\lambda) d\lambda}{\int_{280}^{320} d\lambda} \quad (1)$$

$$\text{UVA blocking } (\%) = 100 - \frac{100 \int_{320}^{400} T(\lambda) d\lambda}{\int_{320}^{400} d\lambda} \quad (2)$$

In which, T(λ) refers to the film average transference at the wavelength λ, and dλ specifies the coatings bandwidth. UV-visible transmittance curves are portrayed in Figure 8 to investigate the resistance against UV rays and transfer of the visible light induced by the films. PUA film blocks the rays with short wavelength in UVC range (220-280 nm), but suggests a feeble protective function in UVB region (280-320 nm), and in UVA area (320-400 nm), it evinces very weak performance to absorb UV radiation and consequently, a big portion of UV rays can pass through it.

However, PUA/CQDs film offers a great capacity to absorb and block the UV rays in a manner that UV absorption by PUA/CQDs in the UVB and UVA regions are respectively 99.35% and 99.15%. Thus, PUA/CQDs is considered a UV protective coating owing to capability of blocking higher than 99% of UV rays.

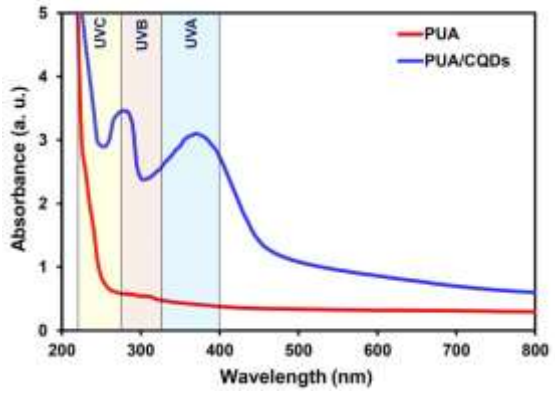

Fig. 7. UV-vis curves of PUA and PUA/CQDs coatings.

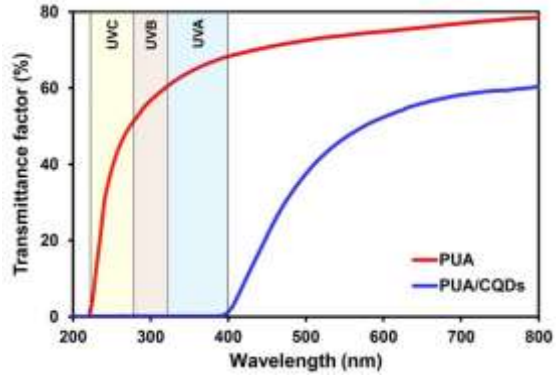

Fig. 8. UV-vis transmittance curves of PUA and PUA/CQDs coatings.

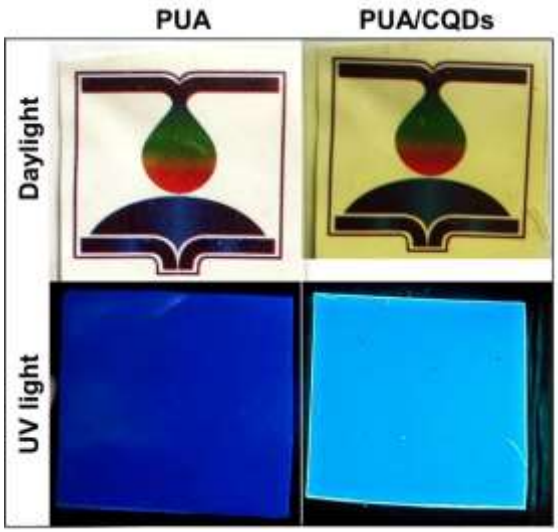

Fig. 9. Images of PUA and PUA/CQDs coatings under (a) daylight and (b) UV light.

Figure 9 portraits images of PUA and PUA/CQDs films exposed to daylight and the UV light. PUA offers a transparent appearance lacking color open to daylight. By loading CQDs with 0.5 wt % concentration, although it changes to a light brown color, partially keeps the lucid face. PUA film before the UV light with 365 nm wavelength appears to be purple, while PUA/CQDs film is lighter confirming fluorescence response and intense UV absorption.

3.5. Anti-corrosive properties of PUA and PUA/CQDs coatings

EIS and salt spray tests were performed to examine resistance of the coatings against corrosion. To execute the EIS test, the PUA and PUA/CQDs coatings applied to steel surface floated in NaCl 3.5% solution for 10 days.

As Figure 10 depicts, bode curves indicate remarkable changes for impedance value at low frequencies. Impedance at low frequency implies a total impedance of working electrode system of coating-metal and includes coating resistance and charge transfer resistance [48]. By loading CQDs 0.5 wt% into polymer matrix, the total impedance of working electrode at low frequencies increases, in a manner that at 1.0-01E (0.1) Hz frequency, the total impedance of electrode grows by 8.55+09E ohm.cm^2. The resulted change proves that a defensive coating has been created on the electrode surface and accordingly, protects it more from chloride ions access.

Nyquist curves are described in Figure 11. The appeared semicircles signify the change transfer and double layer capacitance occurred during formation of the prime films. The capacitive loop with bigger diameter is related to PUA/CQDs suggesting better performance of hindering against corrosive agents. Impedance rises along with adding CQDs 0.5 wt% to the polymer matrix implying the created coating on the steel surface (steel-PUA/CQDs) evinces higher resistance to corrosion compared to PUA coating (steel-PUA). Chloride ions make a hole like corrosion and accelerate the total corrosion of the steel surfaces [49, 50]. The corrosive factors such as chloride ions in PUA penetrate into the coating

vigorously and this way, the corrosion process intensifies. CQDs uniform dispersion throughout the polymer matrix, filling in the polymer holes with CQDs and constitution of hydrogen bonds and van der Waals intermolecular forces in the steel-PUA/CQDs interface bring about strong adhesion and regarding this, resistance is augmented.

The function of the coatings against corrosion was estimated relying upon the rusting intensity and scribe failure according to ASTM standard with D1654-05 to assess the scribe failure extreme including a 0-10 evaluation range, in a way that 0 implies the coatings with the highest degree of scribe failure and 10 represents the scribe free coatings, and ASTM D610-01 standard relates to analysis of the rusting intensity. Moreover, ASTM standard of D714-02 was taken into account to determine the blisters quality using 0 to 10 even numbers, with 2 for the samples offering the highest blisters and 10 for those without blister. Results from salt spray testing are displayed in Figure 12(a) and Table 2. About PUA, visual evaluation of the photographic reference standards proves the growth of rusting extreme on the scratched surface versus PUA/CQDs. It seems that the holes numbers and the polymer free spaces are high in PUA and corrosive factors can more easily penetrate into the coating; as a result, corrosive factors push themselves to the metal surface in a short time and start to destroy it [51]. In PUA/CQDs nanocomposite contrary to PUA, a part of holes and free spaces are filled in with CQDs, thus, due to long distance to penetration, resistance to corrosion is improved. Additionally, CQDs can entrap the scattered oxygen molecules in the damaged region of the coating and reduce them and based on this, interrupt the corrosion process in the scratched region. Figure 12(b) furnishes schematic corrosion mechanism of the PUA/CQDs coating toward corrosive agents.

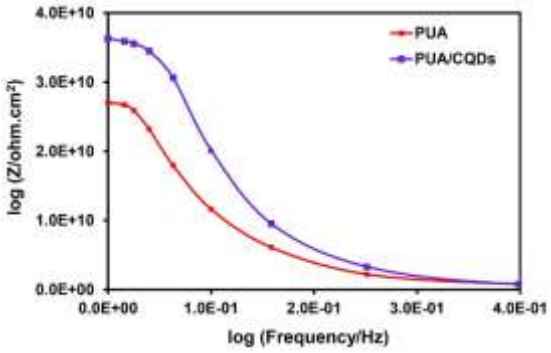

Fig. 10. Bode curves of PUA and PUA/CQDs coatings.

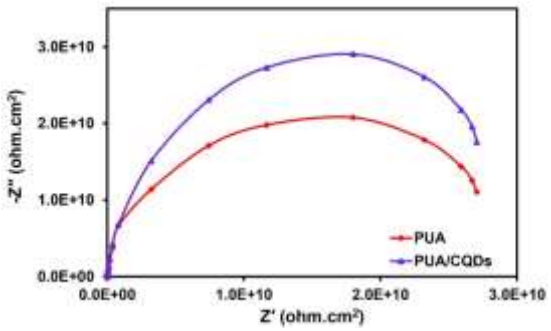

Fig. 11. Nyquist curves of PUA and PUA/CQDs coatings.

Table 2. Anti-corrosive performance of PUA and PUA/CQDs coatings

Coatings	Scribe failure	Rust grades	Blistering size
PUA	4	4	4
PUA/CQDs	6	6	4

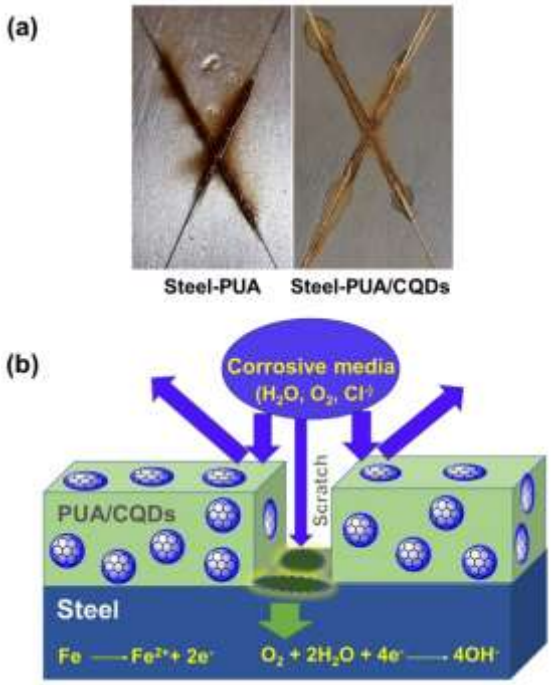

Fig. 12. (a) Images of resistance to corrosion for steel-PUA and steel-PUA/CQDs coatings and (b) schematic anti-corrosive mechanism of PUA/CQDs coating against corrosion.

3.6. Comparison with previous studies

Table 3 depicts the data from current research compared to the two previous works. These findings are approximately similar to the former findings. In the current work, weight percentages of CQDs were different from the former works and lower weight percentages of CQDs loaded into polymer matrix were selected to make a comparison [38, 51]. One can conclude that a good dispersion and non-agglomeration of CQDs particles in polymer matrix could meet a part of needs for reinforcement current nanocomposite coating.

Table 3. Current work (PUA/CQDs) compared to previous works.

Methods	PUA/CQDs	[51]	[38]
Pull-off adhesion strength	2.64 (MPa)	2.45 (MPa)	1.85 (MPa)
FL emission	470 (nm)	470 (nm)	435 (nm)
UV-blocking	99%	98%	95%
Anti-corrosion properties	6, 4 (Rust grades)	6, 5 (Blistering size)	-

4. Conclusion

In the current research work, bio-based UV-curable coatings were synthesized. To prepare polyurethane acrylate oligomer, castor oil was employed as a natural and biocompatible polyol. CQDs characterization and strengthening effect upon thermal stability, adhesion strength, fluorescence properties, UV-absorption and UV-blocking, and resistance to corrosion in these coatings were judged by different tools and spectroscopy techniques. Findings confirmed that adding CQDs (0.5 wt%) to the polymer matrix elicited a 0.76 MPa growth of adhesion strength in addition to an increase in thermal stability at higher temperatures. On the other hand, PUA/CQDs emitted blue fluorescence at 470 nm and evinced strong UV absorption in all of the UV regions (225, 280 and 365 nm), in a manner that this film could block higher than 99% of UV rays. Salt spray test and EIS analysis (based on Bode and Nyquist curves) validated increase in resistance to corrosion in PUA/CQDs film in contrast with PUA (blank) film. Considering this, CQDs as a nano-strengthening agent can enhance the resistance of nanocomposite coating against corrosive causes. Therefore, CQDs can be an appropriate candidate to produce nanocomposite coatings with ability of resistance to UV radiation and to protect the metal surfaces from corrosion damage, and accordingly could be widely employed in petroleum, petrochemical, electronic, aircraft and automotive industries.

Declaration of interests

No conflict of interests found in the whole process of this work conduct; the authors approved.

Funding

The authors claimed this work was done completely without any financial support.

References

[1] alavi Nikje, M.M., Zarghami, H. (2020). Investigation of the Mo/MgO hybrid catalytic effect of the recycling of flexible polyurethane foam, *Appl Chem Today*, 15(55), 221-234.

[2] Das, S., Pandey, P., Mohanty, S., et al. (2017). Investigation into the Influence of UV Aging on Green Polyurethane/Nanosilica Composite Coatings Based on Transesterified Castor Oil and Palm Oil Isocyanate. *J Inorg Organomet Polym*, 27, 641-657.

[3] Atabaki, F., Razaghpoor, S., jahangiri, S. (2019). Synthesis of poly(urethane-urea)s based on novel macro-diamines: enhanced mechanical properties, *Appl Chem Today*, 14(53), 11-20.

[4] Madhi, A., Shirkavand Hadavand B. (2021). Tri-functional Bio-friendly Cross-linker for UV-Curable Coatings: Synthesis and Study of

Viscoelastic Properties. *Prog. Color Color. Coat*, 14(3), 199-207.

[5] Azizi, M., Seyed Dorraji, M. S., Rasoulifard, M. (2018). Preparation of polyurethane nanofibers containing cefixime trihydrate: in vitro release kinetic studies, *Appl Chem Today*, 13(46), 239-248.

[6] Yuan, Y., Chen, M., Zhou, Q., Liu, R. (2019). Synthesis and properties of UV-curable cardanol-based acrylate oligomers with cyclotriphosphazene core. *J. Coat. Technol. Res*, 16:179-88.

[7] Madhi, A., Shirkavand Hadavand, B., Amoozadeh, A. (2017). Synthesis, characterization and study on thermal stability, mechanical properties and thermal conductivity of UV-curable urethane acrylate-Clay (MMT) nanocomposites. *Appl Chem today*, 12(45), 91-98.

[8] Papageorgiou, G.Z. (2018). Thinking Green: Sustainable Polymers from Renewable Resources. *Polymers (Basel)*, 10(9), 952.

[9] Malani, R.S., Malshe, V.C., Thorat, B.N. (2022). Polyols and polyurethanes from renewable sources: past, present, and future-part 2: plant-derived materials. *J Coat Technol Res*, 19: 361-375.

[10] de Morais, J.P.P., Pacheco, I.K.C., Filho, ALMM., et al. (2021). Polyurethane derived from castor oil monoacylglyceride (Ricinus communis) for bone defects reconstruction: characterization and in vivo testing. *J Mater Sci: Mater Med*, 32, 39.

[11] Lee, J.H., Kim, S.H., Oh, K.W. (2021). Bio-Based Polyurethane Foams with Castor Oil Based Multifunctional Polyols for Improved Compressive Properties. *Polymers*, 13: 576.

[12] Lee, Y.J., Park, C.K., Kim, S.H. (2018). Fabrication of castor-oil/polycaprolactone based bio-polyurethane foam reinforced with nanocellulose. *Polym Compos*, 6, 2004-11.

[13] Lu, T., Solis-Ramos, E., Yi, Y., Kumosa, M. (2018). UV degradation model for polymers and polymer matrix composites. *Polym. Degrad. Stab*, 154, 203-10.

[14] Peng, L., Lin, M., Zhang, S., Li, L., Fu, Q., Hou, J. (2019). A Self-Healing Coating with UV-Shielding Property. *Coatings*, 9: 421.

[15] Liu, H., Hu, D., Chen, X., Ma, W. (2021). Surface engineering of nanoparticles for highly efficient UV-shielding composites. *Polym Adv Technol*, 1, 6-16.

[16] Deng, H., Xie, F., Shi, H., Li, Y., Liu, S. (2022). Zhang C. UV resistance, anticorrosion and high toughness bio-based waterborne polyurethane enabled by a Sorbitan monooleate. *Chem. Eng. J*, 446, 137124.

[17] Zhu, Y., Zhang, X., Zhang, L., Hu, L., Zhang, F., Wang, Y., Ding, Y., Zhu, X., Yang, W. (2022). Membranes constructed with zero-dimension carbon quantum dots for CO_2 separation. *J. Membr. Sci*, 664:1 21086.

[18] Madhi, A., Shirkavand Hadavand, B. (2022). Chemical treatment of cotton fabric by eco-friendly carbon quantum dots-chitosan nanocomposites. *Appl Chem today*,17(63), 55-66.

[19] Sousa, H.B.A., Martins, C.S.M., Prior, J.A.V. (2021). You Don't Learn That in School: An Updated Practical Guide to Carbon Quantum Dots. *Nanomaterials (Basel)*, 11(3), 611.

[20] Tabaraki, R., Sadeghi nezhad, N., Yousefi poor, S. (2018). Green fluorescent sensor based

on carbon quantum dots for Cr(VI) determination, *Appl Chem Today*, 13(48), 339-350.

[21] Madhi, A., Shirkavand Hadavand, B., Madhi, A. H. (2024). Bio-friendly fluorescent polyvinyl alcohol/gelatin/chitosan hydrogel membranes strengthened by g-C_3N_4/CQDs nanocomposite: Preparation, investigation of UV-absorption, mechanical and rheological properties, *Fuller. Nanotub. Carbon Nanostructures*, 32, 1-10. DOI: 10.1080/1536383X.2024.2310697.

[22] Madhi, A., Shirkavand Hadavand, B. and Madhi, M. H. (2024). Smart fluorescent PVA/CS/AV/g-C_3N_4QDs hydrogel nanocomposites: synthesis and study of UV absorbance, rheological and self-healing properties, *Fuller. Nanotub. Carbon Nanostructures*, 32, 1-11. DOI: 10.1080/1536383X.2024.2331779

[23] Das, P., Ganguly, S., Ahmed, S.R., Sherazee, M., Margel, S., Gedanken, A., Srinivasan, S., Rajabzadeh, A.R. (2022). Carbon dot biopolymer-based flexible functional films for antioxidant and food monitoring applications. *ACS Appl. Polym. Mater*, 4(12), 9323-9340.

[24] Kausar, A., Ahmad, I., Eisa, M.H., Maaza, M. (2023). Avant-Garde Polymer/Graphene Nanocomposites for Corrosion Protection: Design, Features, and Performance. *Corros. Mater. Degrad*, 4, 33-53.

[25] Hegde, M., Kavanagh, Y., Duffy, B., Tobin, E.F. (2022). Abrasion and Cavitation Erosion Resistance of Multi-Layer Dip Coated Sol-Gel Coatings on AA2024-T3. Corros. Mater. *Degrad*, 3, 661-671.

[26] Bhattacharya, M. (2016). Polymer nanocomposites-A comparison between carbon nanotubes, graphene, and clay as nanofillers. *Materials*, 9, 262.

[27] Muresan, L.M. (2023). Nanocomposite Coatings for Anti-Corrosion Properties of Metallic Substrates. *Materials (Basel)*, 16(14), 5092.

[28] Reda, Y., Abdelbar, M., El-Shamy, A.M. (2021). Fortification performance of polyurethane coating in outdoor historical ironworks. *Bull Natl Res Cent*, 45, 69.

[29] El-Shamy, O.A. and Deyab, M.A. (2023). Novel anticorrosive coatings based on nanocomposites of epoxy, chitosan, and silver. *Maters Lett*, 330, 133298.

[30] Ghasemi, D., Rouhollahi, A., Rasouli, F. (2020). Synthesis and optimization of composite coatings based on electrical conductive of polyaniline and polyindole for anti-corrosion protection of carbon steel, *Appl Chem Today*, 15(54), 331-336.

[31] Eslamizadeh, H., Mohammadi, A., Mohammadi, S. (2023). Preparation of new Schiff bases based on thiosemicarbazide and evaluation of their inhibitory properties on corrosion of carbon steel in acidic environment, *Appl Chem Today*, 18(66), 99-124.

[32] Abdolmaleki, M., Golbedaghi, R., Ahmadieh, S. (2021). Synthesis of Ni-W/SiO_2 nanocomposite coatings and investigation of their corrosion behavior in 3.5 % NaCl solution, *Appl Chem Today*, 16(59), 51-62.

[33] Shabani-Nooshabadi, M., Karimian-Taheri, F., Jafari, Y. (2016). Evaluation of anti-corrosion properties of electrosynthesized

polyaniline on copper at various immersion times, *Appl Chem Today*, 11(40), 33-54.

[34] Pouretedal, H. R., Azimi, A., Mahbob, S. (2023). The effect of ethylene glycol and diethylene glycol additives on the quality of nickel coating on stainless steel substrate by electrodeposition method, *Appl Chem Today*, 18(68), 145-160.

[35] Di, Z., Zhao, Q., Xu, H., Wu, K., Yan, Y., Jin, X., Shen, H., Lv, Y., Ran, B. (2022). N-doped Carbon Quantum Dots with Mechanical Enhancement and Fluorescence Properties Toward Anti-Corrosion Coating. *Int. J. Electrochem. Sci*, 17, 2212101.

[36] Wang, J., Du, P., Zhao, H., Pu, J., Yu, C. (2019). Novel nitrogen doped carbon dots enhancing the anticorrosive performance of waterborne epoxy coatings. *Nanoscale Adv*, 1(9), 3443-51.

[37] Feng, C., Zhu, L., Chen, L., Hui, X., Liu, J., He, L., Bai, X., Yu, Z. (2023). A High-Performance Anti-Corrosive Epoxy Coating Based on Ultra-Thin Hydroxyapatite Nanosheets with pH-Responsive Functions. *Molecules*, 28, 6223.

[38] Madhi, A., Shirkavand Hadavand, B. (2022). UV protective bio-based epoxy/carbon quantum dots nanocomposite coatings: Synthesis and investigation of properties. *J Compos Mater*, 56(14), 2201-2210.

[39] Choi, W-C., Gavande, V., Kim, D-Y., Lee, W-K. (2023). Study on Press Formability and Properties of UV-Curable Polyurethane Acrylate Coatings with Different Reactive Diluents. *Polymers*, 15, 880.

[40] Phetcharee, K., Sirisit, N., Manyam, J., Paoprasert, P. (2021). Highly sensitive Ni^{2+} sensors based on polyurethane-derived, label-free carbon dots with high adsorption capacity. *ChemistrySelect*, 6(31), 7964-71.

[41] Cao, B.H., Chen, W., Wei, W.Y., Chen, Y.L., Yuan, Y. (2021). Carbon dots intensified mechanochemiluminescence from waterborne polyurethanes as tunable force sensing materials. *Chin J Polym Sci*, 39, 1403-1411.

[42] Madhi, A., Shirkavand Hadavand, B. (2020). Bio-based UV-curable urethane acrylate graphene nanocomposites: synthesis and properties. *SN Appl. Sci*, 2, 724.

[43] Hirn, U., Schennach, R. (2015). Comprehensive analysis of individual pulp fiber bonds quantifies the mechanisms of fiber bonding in paper. *Sci Rep*, 5, 10503.

[44] Madhi, A., Shirkavand Hadavand, B., Madhi, A.H. (2023). Environmentally friendly g-C_3N_4/carbon quantum dots nanocomposites as fluorescent and anti-spoofing inks. *Fuller. Nanotub. Carbon Nanostructures*, 31(10), 953-960.

[45] Madhi, A. (2023). Green fluorescent unsaturated polyester/graphitic carbon nitride quantum dots nanocomposites: Preparation and study of UV-resistance, mechanical and viscoelastic properties. *J Compos Mater*, 57(15), 2437-2450.

[46] Khan, A., Ezati, P., Rhim, J.W. (2023). Chitosan/Starch-Based Active Packaging Film with N, P-Doped Carbon Dots for Meat Packaging. *CS Appl. Bio Mater*, 6(3), 1294-1305.

[47] Bae, G., Ahn, C., Jeon, S. (2021). Transparent polymer nanocomposite with three-dimensional ZnO thin-shell with high

UV-shielding performance. *Funct. Compos. Struct*, 3: 025007.

[48] Zhang, Y., Zhao, M., Zhang, J., Shao, Q., Li, J., Li, H., Lin, B., Yu, M., Chen, S., Guo, Z. (2018). Excellent corrosion protection performance of epoxy composite coatings filled with silane functionalized silicon nitride. *J Polym Res*, 25, 130.

[49] Zhang, B., Wang, J., Wu, B., Guo, X.W., Wang, Y.J, Chen, D., Zhang, Y.C., Du, K., Oguzie, E.E., Ma, X.L. (2018). Unmasking chloride attack on the passive film of metals. *Nat. Commun*, 9, 2559.

[50] Ahmed, S., Hou, Y., Lepkova, K., Pojtanabuntoeng, T. (2023). Investigation of the Effect Chloride Ions on Carbon Steel in Closed Environments at Different Temperatures. *Corros. Mater. Degrad*, 4, 364-381.

[51] Madhi, A. (2023). Smart epoxy/polyurethane/carbon quantum dots hybrid coatings: Synthesis and study of UV-shielding, viscoelastic, and anti-corrosive properties, *Polym-Plast Technol Eng*, 62(4), 403-418.